

Quantification of Solubility Trapping in Natural and Engineered CO₂ Reservoirs

Rory Leslie^{1*}, Andrew J. Cavanagh¹, R. Stuart Haszeldine^{1,2}, Gareth Johnson³ and Stuart M.V. Gilfillan¹

¹School of GeoSciences, Grant Institute, University of Edinburgh, Edinburgh, EH9 3FE, UK

²SCCS, High School Yards, Infirmary Street, Edinburgh, EH1 1LZ, Scotland

³Department of Civil and Environmental Engineering, University of Strathclyde, Glasgow, G1 1XZ, UK

* Correspondence address: rory.leslie@ed.ac.uk

Solubility Trapping Nat. & Eng. CO₂ Res.

Abstract: Secure retention of CO₂ in geological reservoirs is essential for effective storage. Solubility trapping, the dissolution of CO₂ into formation water, is a major sink on geological timescales in natural CO₂ reservoirs. Observations during CO₂ injection, combined with models of CO₂ reservoirs, indicate the immediate onset of solubility trapping. There is uncertainty regarding the evolution of dissolution rates between the observable engineered timescale of years and decades, to the >10 kyr state represented by natural CO₂ reservoirs. A small number of studies have constrained dissolution rates within natural analogues. The studies show that solubility trapping is the principal storage mechanism after structural trapping, removing 10–50% of CO₂ across whole reservoirs. Natural analogues, engineered reservoirs and model studies produce a wide range of estimates on the fraction of CO₂ dissolved and the dissolution rate. Analogue and engineered reservoirs do not show the high fractions of dissolved CO₂ seen in several models. Evidence from natural analogues supports a model of most dissolution occurring during emplacement and migration, before the establishment of a stable gas-water contact. A rapid decline in CO₂ dissolution rate over time suggests that analogue reservoirs are in dissolution equilibrium for most of the CO₂ residence time.

Supplementary material: [All data used in this paper are contained in the supplementary information spreadsheet included with the submission. A doi and permanent url do not exist. Therefore, we wish to use the GSL figshare portal]

51 CO₂ trapping mechanisms are physical and chemical processes that prevent CO₂ from migrating out of
52 a reservoir. For CO₂ capture and storage (CCS), trapping is the key to secure and long-term
53 sequestration of CO₂ (Alcalde *et al.* 2018; Miocic *et al.* 2018). Structural and stratigraphic trapping
54 beneath a seal, such as a shale caprock, and residual trapping in the reservoir pores through which
55 the CO₂ migrates, are essential components of the initial storage. Depending on storage depth,
56 injected CO₂ exists as a gas, liquid or supercritical phase. We use the term ‘free-phase’ to refer to CO₂
57 in the gas, liquid or supercritical phases to differentiate it from aqueous CO₂ dissolved in formation
58 water. CO₂ dissolution, also called solubility trapping, can remove free-phase CO₂ over time (Ajayi *et al.*
59 *et al.* 2019). Formation water has the potential to store up to 50 kg/m³ of dissolved CO₂ when fully
60 saturated at reservoir conditions of 37°C and 100 kbar. The 37°C and 100 kbar reservoir conditions
61 approximate the Utsira Formation at the Sleipner storage reservoir and are typical of offshore sites
62 considered for saline aquifer storage (Steel *et al.* 2016). CO₂-saturated formation water is slightly
63 denser than ambient formation water and sinks in the reservoir. Naturally occurring CO₂ reservoirs
64 can be used as analogues for understanding processes, such as solubility trapping, over geological
65 timescales (Allis *et al.* 2001; Haszeldine *et al.* 2005). Solubility trapping is significant in these analogue
66 reservoirs (Gilfillan *et al.* 2009; Zhou *et al.* 2012). In the widely cited Bravo Dome CO₂ field (Sathaye *et al.*
67 *et al.* 2014; Zwahlen *et al.* 2017) solubility trapping has removed between 10–50% of the 1600–1800
68 million metric tonnes (Mt) of CO₂ originally emplaced.

69

70 The physics and chemistry of CO₂ dissolution in storage reservoirs are well understood. Increased
71 pressure increases solubility; while increased temperature and salinity reduce solubility (Spycher &
72 Pruess 2005; Pruess & Spycher 2007; Riaz & Cinar 2014; Jacob & Saylor 2016). Pre-injection formation
73 water may contain dissolved CO₂, in equilibrium with carbonate minerals. Injection of free-phase CO₂
74 increases the partial pressure of CO₂ in the reservoir. The increased fugacity of the CO₂ would,
75 according to Henry’s Law, cause dissolution of the CO₂ into the formation water (Majer *et al.* 2008).
76 Dissolution will stop when a new equilibrium is reached. Knowledge of the formation water volume,
77 salinity, initial CO₂ saturation, reservoir pressure and temperature allows for a good approximation of
78 the potential maximum mass of dissolved CO₂.

79

80 Free-phase CO₂ and water are immiscible (Newmark *et al.* 2010). At the storage reservoir scale (>1
81 km), the CO₂ dissolution rate is effectively controlled by the surface-area of the free-phase CO₂ plume
82 and by CO₂ mobility, which allows contact with formation water. Capillary action, viscous flow,
83 pressure and gravity control the migration of the CO₂ plume in the reservoir. Molecular diffusion of
84 CO₂ within the formation water causes very low rates of dissolution (Pruess & Nordbotten 2011) but
85 can persist after emplacement and stabilisation of the CO₂ plume. Diffusion may be the main process
86 facilitating CO₂ dissolution over geological timescales in reservoirs where density-driven convection
87 does not occur. If the Rayleigh number, primarily controlled by reservoir permeability, is sufficiently
88 high, then density-driven convection may initiate at the front of the migrating CO₂ plume. The
89 convection is driven by the increased density of CO₂-saturated formation water relative to ambient
90 formation water. Convection enhances dissolution rates by circulating more CO₂-saturated formation
91 water away from the plume and less CO₂-saturated formation water towards the plume (Ajayi *et al.*
92 *et al.* 2019). Since convection accelerates the volume of formation water contacted, it increases the rate of
93 CO₂ dissolution (Pruess & Nordbotten 2011). Convection may continue after stabilisation of the CO₂
94 plume and enhance long-term dissolution rates compared to diffusion-only scenarios. In a closed
95 system, convection will still result in the same mass of CO₂ dissolved. In reservoirs with aquifer flow
96 (advection), the total mass and rate of CO₂ dissolution will be higher, since the total volume and rate
97 of formation water contacting the CO₂ is higher.

98

99 The total mass and rates of CO₂ dissolution in engineered sites are debated. Estimates of dissolution
100 can vary widely due to the large number of site-specific variables (e.g. permeability, anisotropy,
101 heterogeneity) and fluid dynamics (diffusion, convection, and advection) which are difficult to

102 accurately quantify. Some authors have attempted universal algorithmic formulations that capture
103 the expected behaviour (e.g. Martinez & Hesse 2016), while others have demonstrated the
104 adaptability of numerical reservoir simulators to estimate outcomes for specific case studies (e.g.
105 Pickup *et al.* 2011).

106
107 In natural CO₂ reservoirs, large volumes of CO₂ have been trapped in sedimentary rocks on geological
108 timescales. Commonly cited examples of commercially exploited CO₂ accumulations from the
109 Colorado Plateau, Rocky Mountains and Gulf Coast regions of the USA have undergone detailed
110 geochemical studies (Allis *et al.* 2001, Gilfillan *et al.* 2008; Gilfillan *et al.* 2009; Zhou *et al.* 2012). Results
111 from geochemical studies can help inform modelling studies of CO₂ dissolution and provide a
112 comparison with measurements from operational CCS sites to better calibrate predictive models of
113 long-term solubility trapping. Here, we focus on using natural analogues to complement studies of
114 solubility trapping using modelling and observations from engineered CO₂ reservoirs. We examine
115 both the total dissolved CO₂ mass and dissolution rate with a focus on timescales that cannot be
116 observed in operational settings, i.e. 10² to 10⁴ years.

117 118 **Aims and hypotheses**

119
120 This study has three aims: first, to review the work on solubility trapping from previous natural
121 analogue studies. Second, to assess the value of natural analogues as a means of investigating long-
122 term solubility trapping in CCS reservoirs. And third, to test conceptual scenarios of solubility trapping
123 rate over time using results from analogues, engineered reservoirs and models.

124
125 In terms of the third aim, there is uncertainty on the relative contribution of dissolution during the
126 injection and post-injection phases of engineered storage. The injection phase is defined as the initial
127 years-to-decades of a CCS project when CO₂ injection is occurring. The post-injection phase refers to
128 the decades of post-injection monitoring followed by the centuries and millennia of long-term storage
129 (>10 kyr). In the post-injection phase, a stable, structurally trapped CO₂ plume would be expected to
130 develop under a caprock in most reservoir settings. Even in well-described reservoirs, the CO₂
131 dissolution rate and the potential occurrence of equilibrium points are uncertain. The range of
132 outcomes can be summarised by two end-member scenarios for the relative rates of solubility
133 trapping from the start of injection, through to long-term storage (Fig. 1).

134
135 Scenario A can be considered the ‘rapid decline’ dissolution scenario (Fig. 1a). Dissolution rates are
136 initially very high at the start of injection but decline exponentially. In terms of process, this involves
137 rapid mixing of the injected CO₂ plume with formation water by entrapment and displacement. In
138 scenario A an equilibrium point is reached in the post-injection phase. Equilibrium occurs because of
139 the lowered CO₂ fugacity, due to the reduced free-phase volume, and the high CO₂ saturation of the
140 surrounding, hydrostatic formation water. Mineral dissolution and precipitation reactions associated
141 with CO₂ are also in equilibrium. Unless the system is disturbed, the dissolution rate beyond the
142 equilibrium point is zero.

143
144 Scenario B can be considered the ‘steady decline’ dissolution rate scenario (Fig. 1b). Dissolution rates
145 are still highest during injection and occur through the same processes as in scenario A; however, the
146 exponential rate of decay is slower. This is due to diffusion, and potentially convection, persisting
147 throughout the post-injection period. The continued action of these processes over thousands to
148 millions of years results in a delayed equilibrium of the system and a larger mass of CO₂ dissolved.

149
150 The occurrence of equilibrium points and the potential persistence of processes like diffusion and
151 convection are influenced by reservoir properties. Different forms of anisotropy and heterogeneity
152 can variably influence dissolution. Uniformly high permeability will enhance plume advancement and

153 enable convection, while the occurrence of low-permeability layers will increase the CO₂-formation
 154 water contact area due to CO₂ channelling and capillary effects (Gilmore *et al.* 2020). Different spatial
 155 orders of reservoir heterogeneity may variably enhance or inhibit the development of convection
 156 (Soltanian *et al.* 2017). Hydrological variables such as the aquifer size and advection will also have
 157 effects that are difficult to quantify. The interplay between factors means that, even with quality
 158 datasets, a basic prediction of scenario A or scenario B-like behaviour in a CCS reservoir is challenging.
 159 Analysis of existing data from the study of natural CO₂ storage analogues and the comparison of
 160 numerical and analytical modelling studies can allow the applicability of the end-member scenarios to
 161 be tested.

162

163 **Dissolution in engineered CCS sites**

164

165 Sleipner, the world's longest running engineered CO₂ storage site, is located in the Norwegian sector
 166 of the North Sea. Since injection began in 1996, over 18 million metric tons of CO₂ have been stored
 167 to date (Williams & Chadwick 2021). As the longest running engineered CO₂ storage site with a large
 168 geophysical monitoring dataset, it provides a decadal timescale estimate of physical and geochemical
 169 trapping.

170

171 The Miocene-Pliocene age Utsira Formation aquifer at Sleipner has high porosity and permeability of
 172 35% and 2 darcy. The Utsira Formation is approximately 300 m thick and composed of 90% net
 173 sandstone, vertically segregated by thin sub-horizontal mudstone beds, which allow for a stacked
 174 vertical migration and structural trapping of the CO₂ (Eiken *et al.* 2011; Cavanagh & Haszeldine 2014).

175

176 Seabed gravimetry has been the primary means of estimating dissolution rates (Alnes *et al.* 2011) as
 177 the absence of reservoir fluid sampling means that other established geochemical techniques cannot
 178 be used (Cavanagh 2013). An initial seabed gravimetric survey was acquired in 2002, after 5 million
 179 Mt of CO₂ had been injected. Repeat surveys were acquired in 2005, after 8 Mt had been injected, and
 180 in 2009, after 11 Mt had been injected. Analysis of the data focussed on determining the density of
 181 the CO₂ plume (Nooner *et al.* 2007; Alnes *et al.* 2008). The gravity estimated plume density was
 182 compared with the expected CO₂ density from reservoir temperature and pressure conditions, to
 183 estimate the proportion of CO₂ dissolved. An upper estimate of the rate of dissolution was 1.8% per
 184 year (Alnes *et al.* 2011), equivalent to 13% of the total plume mass in 2009. This rate is broadly similar
 185 to the results of independent reactive transport simulation studies which estimated that, by 2011,
 186 10% of the injected CO₂ had dissolved (Chadwick 2013).

187

188 We can compare these two published estimates for Sleipner with a simple analytical approximation
 189 for the mass of CO₂ dissolved during injection. The initial CO₂ saturation of the formation water at
 190 Sleipner was not measured. Here we simplify and assume that the initial formation water is CO₂-free.
 191 In an open aquifer setting the dynamically displaced formation water volume, equivalent to 100% of
 192 the CO₂ volume, is completely saturated given its direct contact with the advancing CO₂ plume front.
 193 An assumed residual formation water pore volume (20% of the plume volume) will also become fully
 194 saturated. Using an average CO₂ plume density of 600 kg/m³ (Cavanagh & Haszeldine 2014), and a
 195 dissolved CO₂ density of 50 kg/m³ for saturated formation water, we estimate that for 11 Mt of
 196 injected CO₂, the rapid dissolution response could be as high as 1.15 Mt (229 kt residual + 917 kt
 197 displaced), which is approximately 10.5% of the injected mass. The estimate is in broad agreement
 198 with the numerical simulation estimate by Chadwick (2013) which also assumes a CO₂-free initial
 199 condition for the formation water. The dissolution estimate using geophysical inversion (Alnes *et al.*
 200 2011) is also in agreement. This suggests that, under observed conditions, the formation water
 201 appears to be free of dissolved CO₂ prior to injection.

202

203 These outcomes indicate significant dissolution at Sleipner during injection. However, the operational
 204 timescales of engineered CO₂ storage sites are short. The short timescales necessitate the
 205 consideration of natural analogues and models to understand the long-term evolution of CO₂ solubility
 206 trapping beyond the injection period.

207

208 **Dissolution in natural analogues**

209

210 Noble gas and stable carbon isotope data acquired from producing CO₂ wells at natural analogue
 211 reservoirs in the USA, Europe, and China, have been used to establish that CO₂ dissolution is the largest
 212 geochemical trapping mechanism over geological timescales, after the primary mechanism of
 213 structural and stratigraphic trapping (Gilfillan *et al.* 2009; Zhou *et al.* 2012). The key gas isotopes within
 214 the CO₂ for identifying and quantifying dissolution are ³He, ⁴He, ²⁰Ne, and δ¹³C.

215

216 The ratio of CO₂ to ³He (CO₂/³He) is used to calculate the fraction of CO₂ that has partitioned from the
 217 free-phase through either dissolution or mineralisation. These partitions are collectively referred to
 218 as free-phase CO₂ removal. CO₂ is soluble in water and reactive with reservoir minerals and dissolved
 219 mineral salts. ³He is present in naturally occurring CO₂ at specific concentrations depending on the
 220 source of the gas. Significantly, ³He is both inert and insoluble in water (Holland & Gilfillan 2013).
 221 Therefore, changes in the free-phase CO₂/³He can be attributed to CO₂ removal at a sampled well
 222 location. Using the highest CO₂/³He sample from a given reservoir as the minimum indication of CO₂
 223 removal, a relative removal fraction in each well can be established. This method suggests that for
 224 Bravo Dome and McElmo Dome, two large natural analogue fields in the USA, portions of the
 225 reservoirs have experienced CO₂ removal of up to 50% at Bravo Dome and up to 90% at McElmo Dome
 226 (Gilfillan *et al.* 2009). These are minimum estimates of CO₂ removal, as they are relative to the highest
 227 CO₂/³He well sample in the field, which itself may have undergone some degree of CO₂ dissolution or
 228 mineralisation.

229

230 Dissolution can be identified as the mechanism of CO₂ removal if decreasing CO₂/³He in the gas sample
 231 correlates with increased ⁴He and ²⁰Ne concentrations. ⁴He and ²⁰Ne originate from different sources
 232 but mix in the reservoir formation water. ⁴He is a by-product of the radioactive decay of U, Th and K
 233 atoms found in many minerals. ²⁰Ne is sourced from the atmosphere through dissolution in meteoric
 234 water and subsequent percolation into deeper formation waters. In gas samples from several
 235 analogue fields, ⁴He and ²⁰Ne share an inverse relationship with CO₂/³He (Gilfillan *et al.* 2009; Zhou *et al.*
 236 *et al.* 2012). As CO₂ dissolution occurs, CO₂/³He in the gas leg decreases. Independently, the ⁴He and ²⁰Ne
 237 concentrations increase due to their partitioning out of the formation water and into the CO₂. Fig. 2
 238 shows a schematic of the isotope ratio variation that is expected within a reservoir due to the
 239 interaction of the CO₂ and water phases.

240

241 Dissolution of CO₂ also causes a predictable δ¹³C fractionation, which is distinct from the fractionation
 242 associated with carbonate mineral precipitation. Therefore, the relationship of δ¹³C to the removal of
 243 free-phase CO₂ is used to quantify the percentage removed through dissolution versus mineralisation.
 244 A study of nine analogue reservoirs found the largest mineralisation contribution to be within the gas
 245 leg of a Bravo Dome well, with up to 18% of CO₂ removal attributed to carbonate precipitation, and
 246 the remaining 82% of CO₂ removal attributed to dissolution (Gilfillan *et al.* 2009). The age of CO₂
 247 emplacement in the studied reservoirs is variable, but commonly >1 Ma. Given the geological age, we
 248 assume that mineralisation has reached equilibrium but the potential for ongoing mineralisation at
 249 slow rates cannot be ruled out.

250

251 Different sources of naturally occurring CO₂, such as magmatism, carbonate dissolution and organic
 252 processes, produce gas with different δ¹³C signatures (Wycherley *et al.* 1999). Mixing of CO₂ sources
 253 with different δ¹³C signatures would complicate the calculation of dissolution and mineralisation. The

254 absolute ³He concentration and CO₂/³He of 6 sampled analogue fields in the USA, including Bravo
255 Dome and McElmo Dome, was within the mantle range (Gilfillan *et al.* 2008; Gilfillan *et al.* 2009). The
256 minor occurrence of carbonate or organic derived CO₂ cannot be ruled out but would be a minor
257 contributor relative to the primary magmatic source. Therefore, a single uniform magmatic source
258 was assumed in all calculations.

259

260 **Analogue studies**

261

262 Bravo Dome is an exceptionally large CO₂ field, containing more than one billion metric tonnes (Gt) of
263 CO₂, which has been in production since 1981. A large gas isotope dataset has been acquired by
264 sampling producing wells. Geochemistry has helped to establish conceptual models of emplacement
265 and original CO₂ mass. The models also estimate the fraction of CO₂ lost to dissolution and, to a first
266 approximation, average long-term dissolution rates. However, the two recently published models of
267 dissolution rates at the field differ because of significantly different age estimates for the CO₂
268 emplacement event (Sathaye *et al.* 2014; Zwahlen *et al.* 2017).

269

270 To the authors' knowledge, Bravo Dome is the only natural analogue where quantitative estimates of
271 dissolved CO₂ mass have been performed. These field studies demonstrate a methodology that could
272 be applied to other analogue reservoirs where gas sampling is possible. Reservoirs where the age of
273 CO₂ arrival is corroborated by multiple independent tests would give more clarity on long-term rates
274 of dissolution.

275

276 Bravo Dome has several features that are atypical of reservoirs considered for CO₂ storage. The
277 gigatonne scale of Bravo Dome is one-to-two orders of magnitude larger than most planned sites.
278 Additionally, the reservoir is highly heterogeneous, under-pressured, and shallow at 700 m below
279 surface (Sathaye *et al.* 2016). The latter two conditions result in a low-density gas phase, whereas
280 engineered sites prefer a denser, super-critical, phase to improve storage capacity. Additionally, a
281 significant area of the reservoir sits directly above an impermeable granitic basement with no gas-
282 water contact (GWC) (Zwahlen *et al.* 2017). The differences hamper a direct comparison with Sleipner,
283 an exemplar of a deep saline aquifer setting (Arts *et al.* 2004).

284

285 Reservoir thickness, porosity, and pre-production pressure mapping provided an estimate of CO₂ mass
286 per unit area. The free-phase CO₂ mass prior to production was estimated to be 1.3 ± 0.6 Gt (Sathaye
287 *et al.* 2014). Mapping CO₂/³He across the field led to estimated free-phase CO₂ removal of 366 ± 120
288 Mt. As mineralisation was shown to be a secondary contributor to free-phase CO₂ removal (Gilfillan
289 *et al.* 2009), the calculations were simplified to attribute all removal to dissolution. By ignoring the
290 removal of CO₂ by mineralisation the results overestimated dissolution at individual sample points by
291 up to 18%. By combining pre-production mass with the calculated dissolved mass, the original
292 emplaced CO₂ mass was estimated to be 1.6 ± 0.67 Gt (Sathaye *et al.* 2014). The error margins for both
293 the original emplaced CO₂ mass and the mass removed through dissolution are large and are primarily
294 caused by variance in reservoir depth (Sathaye *et al.* 2014). The error margins lead to a CO₂ dissolution
295 estimate of 11–52%.

296

297 The calculated mass of dissolved CO₂ can be converted into an average dissolution rate using estimates
298 of emplacement timing. Sathaye *et al.* (2014), assumed that the magmatic CO₂ was sufficiently hot to
299 exceed an apatite closure temperature of 75°C at the reservoir entry point. Age dates of apatite
300 minerals from reservoir core samples were used to constrain the timing of CO₂ emplacement. The
301 method produced an age of 1.2–1.5 Ma, falling within the broad range of 56 ka–1.7 Ma established by
302 dating local igneous rocks proposed to be the source of the magmatic CO₂ (Nereson *et al.* 2013).

303

304 Sathaye *et al.* (2014) assumed that 40% of the total dissolution occurred in the first 5 kyr after
 305 emplacement, followed by much slower dissolution over the remainder of the residence time. This is
 306 similar to our scenario B. The initial phase of relatively fast dissolution is attributed to high capillary
 307 entry pressures in siltstones: during emplacement, Sathaye *et al.* (2014) assumed that CO₂ would have
 308 displaced the formation water in the reservoir sandstones but not the siltstones, leaving a large
 309 volume of unsaturated formation water above the GWC. The CO₂ could saturate the formation water
 310 in the siltstones through diffusion. Based on log data, the average thickness of siltstone layers is less
 311 than 10 m. Sathaye *et al.* (2014) predicted that diffusive transport would fully saturate the siltstones
 312 within 5 kyr. The slower, longer-term dissolution was attributed to diffusion across the stabilised GWC.
 313 In one sector of the field, the authors estimated a dissolution flux greater than that expected for
 314 diffusion and inferred localised density-driven convection to explain the discrepancy.

315
 316 Zwahlen *et al.* (2017) took a different approach, firstly using a higher ³He baseline sample of 7.4×10^9
 317 compared to 5.35×10^9 in Sathaye *et al.* (2014). This results in a larger total emplaced CO₂ mass of 1.8
 318 ± 0.67 Gt and larger free-phase CO₂ removal of 506 ± 166 Mt. The error limits are borrowed from the
 319 Sathaye *et al.* (2014) study, and so remain large. Using the endpoints produced an estimate for CO₂
 320 dissolution of 14–59%.

321
 322 Zwahlen *et al.* (2017) estimated a CO₂ emplacement age of 14–17 ka, based on noble gas and stable
 323 isotope diffusion profiles from the GWC through the gas column. This is much younger than the 1.2–
 324 1.5 Ma estimated by Sathaye *et al.* (2014) and approximately 40 kyr younger than the earliest age date
 325 for local igneous rocks (Nereson *et al.* 2013).

326
 327 The far younger emplacement age and larger estimate of dissolved CO₂ in Zwahlen *et al.* (2017)
 328 produces an average dissolution rate approximately 100 times greater than Sathaye *et al.* (2014)
 329 (Table 1). An explanatory dissolution model was not proposed. However, the dissolution of around
 330 500 Mt of CO₂ in under 20 kyr would require a rapid model, potentially with a significant convection
 331 component, as the diffusive flux rates inferred by Sathaye *et al.* (2014) are insufficient to account for
 332 the estimated dissolution over a much longer timescale.

333
 334 Data from Jackson Dome, Mississippi, another large natural CO₂ reservoir in the USA, supports an
 335 exponential decrease in dissolution rate over time, with the majority of CO₂ dissolution occurring
 336 during the initial migration and emplacement phase. Like the studies from Bravo Dome,
 337 measurements of CO₂/³He were used to determine free-phase CO₂ removal, and $\delta^{13}\text{C}$ data were used
 338 to quantify the role of dissolution versus mineralisation. Greater proportions of dissolution and
 339 increased CO₂-water interaction, indicated by ⁴He and ²⁰Ne, were observed at the field crest compared
 340 to the flanks (Zhou *et al.* 2012). The variation in dissolution from crest to flanks supports a model of
 341 rapid decline in dissolution rate. Due to buoyancy, CO₂ reservoirs fill from the top down. CO₂ trapped
 342 at the crest will have been at the front of the plume and will have displaced the ambient formation
 343 water during migration. High rates of dissolution will have occurred when the CO₂ contacted this
 344 formation water. Later CO₂ charge, which filled the flanks of the reservoir will have had less contact
 345 with under-saturated formation water during migration. CO₂ at the flank, will be in closer proximity to
 346 the GWC, which is established when the plume has stabilised. Despite being closer to the hydrostatic
 347 formation water during storage, the flank samples record less CO₂ dissolution than the crest. This
 348 suggests that diffusion or convection related dissolution, after plume stabilisation, is less significant
 349 than dissolution during the initial emplacement and migration.

350 351 **Modelled dissolution rates**

352
 353 Analytical models and numerical simulations have been used to gain an understanding of the controls
 354 and rates of CO₂ dissolution. These models can be compared with estimates from natural analogues

355 and engineered sites. We have compiled data from eight modelling studies (Table 2) that report
 356 dissolved CO₂ over time (Ozah *et al.* 2005; Pickup *et al.* 2011; Pruess & Nordbotten 2011; Sato *et al.*
 357 2011; Bonneville *et al.* 2013; Szulczewski *et al.* 2013; Kempka *et al.* 2014; Orsini *et al.* 2014). All studies
 358 are reservoir-scale simulations. The smallest 2D simulation included in the analysis has a length of 5
 359 km and a thickness 200 m (Szulczewski *et al.* 2013) and the smallest 3D simulation has a volume of 1
 360 x 10⁹ m³ (Sato *et al.* 2011). All models used realistic generic reservoir properties or were based on
 361 specific prospective or operational storage sites. In some studies, multiple scenarios with different
 362 reservoir properties or model boundary conditions were simulated. In these cases, scenarios
 363 described as a 'reference' or 'base case' were used. In studies without a clear reference case, the
 364 scenario which produced the median case result, in terms of total cumulative dissolution, was
 365 selected. Further details on the selected studies are provided in the supplementary information.

366
 367 Using the model studies, we have calculated the fraction of injected CO₂ that has dissolved and the
 368 average dissolution rates, i.e., the total mass of CO₂ dissolved over the duration of CO₂ residence time.
 369 The dissolution fraction and average dissolution rates allow for a comparison of the conformance of
 370 the Bravo Dome and Sleipner estimates with modelling results. In Fig. 3, the fraction of CO₂ that has
 371 dissolved is plotted against the storage duration time.

372
 373 Dissolution can be normalised to the total mass of CO₂ injected or emplaced to allow for a comparison
 374 of dissolution between scenarios at different scales (Figs. 4 and 5). In Fig. 4, the area of the circles
 375 represents the total mass of CO₂ injected or emplaced in each study. The normalisation resolves the
 376 average fraction of dissolved CO₂ per year relative to the total CO₂ mass. We use the fraction of total
 377 CO₂ dissolved per year as a metric for dissolution instead of dissolution per GWC area. Dissolution per
 378 GWC area does not correctly scale results during the migration phase, because a stable GWC has not
 379 developed, and is further complicated by the variety of different GWC geometries in different
 380 reservoirs. For example, in Bravo Dome only half of the reservoir is in contact with the aquifer, while
 381 in Sleipner multiple stacked contacts within the aquifer are present.

382
 383 Of the eight selected model studies, six reported the change in cumulative dissolved CO₂ over time.
 384 These plots of cumulative dissolved CO₂ were digitised (Rohatgi, 2020) and converted to plots of
 385 dissolution rate over time. These dissolution rate data are normalised to the fraction of total CO₂
 386 dissolved per year and summarised by exponential or power law functions to best fit each study (Fig.
 387 6). The time averaged dissolution rates from natural and engineered CO₂ reservoirs are also plotted
 388 for comparison.

389 **Modelled study results**

390
 391
 392 The model studies included in the analysis show a weak trend of increasing CO₂ dissolution with longer
 393 simulation duration (Fig. 3). The weakness of the correlation reflects the significant variation in many
 394 of the variables that influence dissolution (e.g. boundary conditions, reservoir porosity and
 395 permeability, heterogeneity, fluid pressure and temperature). The Alnes *et al.* (2011) Sleipner
 396 dissolution fraction, after 13 years of storage, fits the middle trend for the model studies. The mid-
 397 case dissolved fractions from the 'young' Bravo Dome estimate of 15.5 ka (Zwahlen *et al.* 2017) and
 398 the 'old' estimate of 13.5 Ma (Sathaye *et al.* 2014) plot below the trend. However, the large error bars
 399 in the Bravo Dome studies mean they could potentially fit a wide range of trends. The two opposing
 400 models for Bravo Dome share a similar range for fraction of CO₂ dissolved, despite the greatly differing
 401 age estimates. Regardless of which Bravo Dome age estimate is assumed to be correct, the results
 402 show that when corrected for scale, total dissolution in Bravo Dome is relatively low when compared
 403 to most equivalent model studies. Even when taking the maximum values from their respective error
 404 ranges, the Bravo Dome studies plot significantly below a group of models predicting higher fractions
 405 of CO₂ dissolved over shorter timescales. Normalising to total CO₂ mass does not fully correct for the

406 decrease in surface area per unit mass of CO₂ in larger scale studies. The lower dissolution percentage
 407 in the Bravo Dome studies are partly due to lower CO₂ surface area- to-CO₂ mass ratios.

408

409 Fig. 4 shows scaled average dissolution rates over the storage and simulation duration with circle areas
 410 equivalent to the total mass of CO₂ injected or emplaced. On the log-log plot there is an approximate
 411 linear trend of reducing dissolution rate with increased storage duration. This trend is expected, as
 412 the variables are related. A relationship of longer storage duration studies considering larger CO₂
 413 masses is also observed. The contrast in circle area illustrates the scale dichotomy of Bravo Dome
 414 relative to Sleipner and most of the model studies. Excluding the analytical study by Szulczewski *et al.*
 415 (2013), the CO₂ masses in Bravo Dome are at least one order of magnitude larger than numerical
 416 model studies. A study where 100% of the CO₂ has dissolved (Szulczewski *et al.* 2013) plots directly on
 417 the upper trend line. Long duration studies whose midpoints plot significantly below the upper line,
 418 such as the two Bravo Dome studies (Sathaye *et al.* 2014; Zwahlen *et al.* 2017), are interpreted to
 419 represent equilibrium being reached with a relatively small fraction of CO₂ dissolved. Shorter duration
 420 studies that show low fractions of dissolution, like the Sleipner gravity study (Alnes *et al.* 2011), can
 421 be partly explained by the short operational timescales. The injected CO₂ is likely not in equilibrium
 422 with the formation water and dissolution is currently ongoing.

423

424 Fig. 5 shows the central cluster of points from Fig. 4 plotted linearly up to 20 kyr. On a scale of linear
 425 time, we observe a non-linear decline in the fraction of CO₂ dissolved per year with increased storage
 426 time. The rate of decline supports a model of rapid initial rates of dissolution, followed by negligible
 427 rates over geological timescales. The common trend of the model studies and the analogue estimate
 428 shows that the models and analogues share similar average dissolution rate versus storage duration
 429 behaviour.

430

431 If a model of rapid dissolution rate decline is favoured, and a steady decline dissolution model
 432 rejected, then calculated dissolution rates from the Bravo Dome analogues can be reconsidered
 433 assuming a significant time-period of equilibrium prior to the samples being collected. The Bravo
 434 Dome studies (Sathaye *et al.* 2014; Zwahlen *et al.* 2017) show similar mid-case estimates of the
 435 fraction of CO₂ dissolved despite the greatly different age estimates. The insensitivity of the fraction
 436 of CO₂ dissolved to the storage duration suggests a significant period of storage time after equilibrium
 437 has been reached in Bravo Dome. Additional time after 14–17 kyr storage duration does not increase
 438 the cumulative dissolved CO₂ and therefore dissolution rates beyond such timescales may be
 439 negligible.

440

441 The potential of dissolution rate reaching equilibrium (i.e. zero dissolution) reframes the apparent
 442 dissolution rate by requiring the inclusion of a stasis period in the calculation. A rapid decline model
 443 for Sleipner (Fig. 1a), would imply that approximately 40% of dissolution occurs during injection
 444 (around 10% of the total injected CO₂), and that dissolution is complete within a few hundred years
 445 (25% of the stored mass), with 80% of the dissolution occurring within 100 years. The alternative, a
 446 steady decline model (Fig. 1b), would initially result in a similar amount of injection related dissolution
 447 (10% of total injected CO₂). A much longer tail to dissolution of around 1000 years results in
 448 approximately 50% of the injected CO₂ dissolving, with 80% of the dissolution occurring after 300
 449 years.

450

451 The scaled dissolution rate over time plots (Fig. 6) show a simplified evolution of the model study
 452 dissolution rates, with a rapid decline over time. The analogue histories are too uncertain to constrain
 453 the onset of stasis, indicating a need for modelling and analogue studies to be combined when
 454 predicting the long-term rate of solubility trapping in CCS storage sites.

455

456 **Discussion**

457

458 The geological CO₂ storage timescales that natural analogues represent will be of interest to many
459 stakeholders. However, it is important to recognise the limitations of analogue studies. The mapping
460 and quantification of subsurface reservoirs is an interpretative and uncertain process due to the
461 relative scarcity of data. Even in ideal settings, the extrapolation of geochemical data between wells
462 entails uncertainty in the estimates of initial CO₂ mass and the fraction dissolved. Bravo Dome is
463 presently the most studied analogue with respect to CO₂ dissolution, but the size, depth, pressure,
464 and gas-water contact configuration are atypical of CCS sites (Sathaye *et al.* 2016). Our synthesis of
465 data suggests that the large size of the reservoir can be partly corrected for, but future studies should
466 focus on analogue sites that more closely represent expected reservoir conditions for CCS sites. This
467 will increase the relevance of analogue results by minimising the influence of atypical factors.

468

469 Greatly differing age estimates have been proposed for Bravo Dome. Sathaye *et al.* (2014) estimate
470 an age of 1.2–1.5 Ma, compared to 14–17 ka proposed by Zwahlen *et al.* (2017). The age uncertainty
471 illustrates a need for analogue sites with well-constrained emplacement timings. At Bravo Dome,
472 there is also a large uncertainty associated with the original emplaced CO₂ mass and dissolved mass,
473 which originates from uncertainty in the reservoir depth and thickness used in the volume calculation.
474 The potentially large errors caused by subsurface uncertainty highlights a need for selecting analogues
475 sites with improved well control and supporting seismic data where available. The simplifying
476 assumption adopted by Sathaye *et al.* (2014) and Zwahlen *et al.* (2017), attributing all removal to
477 dissolution, also introduces an error that can be reduced by considering the CO₂ lost through
478 mineralisation. Ideally, analogue studies require a holistic physical-chemical model for dissolution and
479 mineralisation that can explain the calculated masses and rates. New studies on additional natural CO₂
480 reservoirs would help to better resolve dissolution rates over geological timescales and improve
481 models of CO₂ trapping and storage security in engineered reservoirs.

482

483 At Jackson Dome, CO₂ dissolution is greatest at the reservoir crest and lowest at the flanks (Zhou *et al.*
484 2012). The greater dissolution at the crest suggests that most dissolution occurs during migration
485 and emplacement before the establishment of a stable gas-water contact (GWC). We interpret that
486 the high rates of dissolution during migration and emplacement are because of the mobile plume
487 displacing and mixing with a large volume of formation water that is not fully saturated in CO₂. The
488 significance of GWC proximity and surface-area on dissolution implied by this observation needs to be
489 investigated in more analogue reservoirs. If GWC proximity and surface-area correlate with increased
490 dissolution, this would support a model for sustained, post-emplacement dissolution across the GWC.
491 An inverse correlation would support a model of rapid and early dissolution during the migration and
492 emplacement phase. The occurrence of significant dissolution during migration and emplacement has
493 implications for dissolution rate quantification. A metric in current use is CO₂ flux, i.e. dissolved CO₂
494 mass per GWC contact area per year (g/m²/yr). This metric would be of limited use if most of the
495 dissolution occurs prior to the establishment of a stable gas-water contact.

496

497 Further work on the conceptual model is expected to formalise a two-stage approach that will
498 examine the initial dynamic phase of injection and emplacement and the much longer stabilising phase
499 that follows prior to equilibrium. The significance, and ubiquity of the density-driven convection of
500 CO₂ saturated formation water is not yet established in either phase. The current conceptual model
501 discussed is simple and applies across different reservoirs and injection scenarios. The evolution of
502 dissolution rate over geological time in natural analogues remains highly uncertain and may include a
503 long but elusive stasis phase in hydrostatic settings. Hydrodynamic settings, where a strong aquifer
504 drive is present, will likely require a separate approach. We propose that more research should focus
505 on further quantification of dissolution mass and rate in naturally occurring CO₂ reservoirs that reflect

506 expected regional conditions for areas such as the North Sea, Gulf of Mexico and continental North
507 America.

508

509 The comparison of CO₂ dissolution between analogues, engineered reservoirs and model studies
510 shows a range of behaviour. The results from Sleipner and Bravo Dome do not align with a trend of
511 60–80% solubility trapping within a few thousand years, which some models predict. A potential
512 contributing factor to the lower dissolution in analogue and engineered reservoirs could be small-
513 scale geological heterogeneity influencing diffusion and convection in ways not captured in numerical
514 and analytical simulations. Additionally, the numerical and analytical simulations assume formation
515 water that is initially free from dissolved CO₂. In cases where the initial saturation is unknown and
516 models assume CO₂-free formation water as an initial condition, the results should be interpreted as
517 an upper limit to CO₂ dissolution.

518

519 Our results are relevant to CCS decision makers. Demonstration of significant dissolution of injected
520 CO₂ during a project's operational lifetime would contribute a material increase in the reservoir
521 storage capacity. For example, if approximately 10% of a plume dissolves during injection due to
522 saturation of the displaced plume volume and residual formation water trapped within the plume,
523 this may reduce the required reserves for European CO₂ storage by as much as a gigatonne before
524 2050. Recognition of solubility trapping as an important process could also encourage operators to
525 acquire data on the baseline CO₂ saturation of the reservoir prior to injection. An assayed baseline
526 would allow for a more accurate prediction of solubility trapping. Acquisition of repeat samples, after
527 the start of injection, would allow a confident quantification of solubility trapping on operational
528 timescales.

529

530 **Conclusion**

531

532 Trapping is the essential component of secure CO₂ storage, and solubility trapping makes a significant
533 contribution to the removal of free-phase CO₂ in both natural and engineered reservoirs. Dissolution
534 is likely to remove at least 10% and as much as 50% of the total free-phase CO₂ mass over the lifetime
535 of a storage site.

536

537 Natural CO₂ reservoirs provide insights on the long-term fate of CO₂ in storage reservoirs. CO₂/³He,
538 ⁴He, ²⁰Ne and δ¹³C data from natural CO₂ reservoirs can produce estimates of the CO₂ mass dissolved
539 and the dissolution rate. These data show that solubility trapping removes a significant fraction of
540 free-phase CO₂, thereby enhancing storage security. Quantitative estimates of CO₂ dissolution from
541 Bravo Dome, USA show solubility trapping has removed at least 300 Mt of CO₂ over a minimum of 10
542 kyr.

543

544 Evidence from another North American analogue site, Jackson Dome, supports a model of most
545 dissolution occurring during initial migration and emplacement. Indications from gravimetric data at
546 Sleipner show solubility trapping of around 10% of CO₂, during the operational lifetime of a storage
547 site, i.e. decades. The significance of dissolution of during the initial stages of CO₂ storage means that
548 much of the process is observable during the site's operational period, whereas metrics quantifying
549 CO₂ dissolution by contact area with a stable GWC are less effective, as the stable contact is a post-
550 emplacement feature.

551

552 Analytical and numerical model studies predict a wide range of percentage dissolution. In some cases,
553 dissolution in excess of 60–80% of injected CO₂ is predicted. Such high percentages of dissolution have
554 not been observed on a reservoir-scale at Bravo Dome. Additional studies of natural analogue
555 reservoirs are required to better understand the credible range of dissolved CO₂ mass and CO₂
556 dissolution rate in CCS reservoirs on millennial timescales.

557

558 **Acknowledgements**

559

560 RL is funded by NERC through an E4 DTP studentship NE/S007407/1, and Equinor ASA, with no
 561 influence on the results. AJC and RSH are funded by UKCCSRC2017 EPSRC EP/P026214/1, and RSH by
 562 SCCS (Scottish Funding Council) and HyStorPor EPSRC EP/S027815/1. GJ is funded by the University of
 563 Strathclyde Faculty of Engineering. SMVG is funded by NERC grant NE/R018049/1, EPSRC grants
 564 EP/P026214/1 and EP/K036033/1 and Total E & P, with no influence on results.

565

566 **Author Roles**

567

568 RL wrote most of the article, co-created the figures and carried out the analysis of the data. AJC made
 569 significant contributions to the manuscript, conceptual model and co-created the figures. RSH
 570 critiqued the manuscript and developed the structure of the paper. GJ critiqued the manuscript and
 571 made contributions to the introduction and dissolution in natural analogues sections. SMVG
 572 developed the initial concepts, made significant contributions to the manuscript and secured funding
 573 for the study.

574

575 **Data access statement**

576

577 All data generated or analysed during this study are included in this published article and its
 578 supplementary information files.

579

580 **References**

581

582 Ajayi, T., Gomes, J. S. and Bera, A. 2019. A review of CO₂ storage in geological formations emphasizing
 583 modeling, monitoring and capacity estimation approaches. *Petroleum Science*, **16**, 1028-1063,
 584 <https://doi.org/10.1007/s12182-019-0340-8>

585

586 Alcalde, J., Flude, S., Wilkinson, M., Johnson, G., Edlmann, K., Bond, C. E., Scott, V. Gilfillan, S. M. V.,
 587 Ogaya, X. and Haszeldine, R. S. 2018. Estimating geological CO₂ storage security to deliver on climate
 588 mitigation. *Nature Communications*, **9**, 2201, <https://doi.org/10.1038/s41467-018-04423-1>

589

590 Allis, R., Chidgey T., Gwynn, W., Morgan, C., White, S., Adams, M. and Moore, J. 2001. Natural CO₂
 591 reservoirs on the Colorado Plateau and southern Rocky Mountains: Candidates for CO₂ sequestration.
 592 *In: Proceedings of the First National Conference on Carbon Sequestration*, 14-17 May 2001,
 593 Washington DC, USA.

594

595 Alnes, H., Eiken, O. and Stenvold, T. 2008. Monitoring gas production and CO₂ injection at the Sleipner
 596 field using time-lapse gravimetry. *Geophysics*, **73**, WA155-WA161,
 597 <https://doi.org/10.1190/1.2991119>

598

599 Alnes, H., Eiken, O., Nooner, S., Sasagawac, G., Stenvold, T and Zumberge M. 2011. Results from
 600 Sleipner gravity monitoring: Updated density and temperature distribution of the CO₂ plume. *In: Gale,*
 601 *J., Hendriks, C. and Turkenberg, W. (eds) Energy Procedia*. 10th International Conference on
 602 Greenhouse Gas Control Technologies, 19-23 September 2010, Amsterdam, The Netherlands, **4**, 5504-
 603 5511, <https://doi.org/10.1016/j.egypro.2011.02.536>

604

605 Arts, R., Eiken, O., Chadwick, A., Zweigel, P., van der Meer, L. and Zinszner, B. 2004. Monitoring of CO₂
 606 injected at Sleipner using time-lapse seismic data. *Energy*, **29**, 1383-1392,
 607 <https://doi.org/10.1016/j.energy.2004.03.072>

- 608
609 Bonneville, A., Gilmore, T., Sullivan, C., Vermeul, V., Kelley, M., White, S., Appriou, D., Bjornstad, B., *et*
610 *al.* 2013. Evaluating the Suitability for CO₂ Storage at the FutureGen 2.0 Site, Morgan County, Illinois,
611 USA. *In: Dixon, T. and Yamaji, K. (eds) Energy Procedia*. Proceedings of the 11th International
612 Conference on Greenhouse Gas Control Technologies, 18-22 November 2012, Kyoto, Japan, **37**, 6125-
613 6132, <https://doi.org/10.1016/j.egypro.2013.06.541>
614
- 615 Cavanagh, A. 2013. Benchmark Calibration and Prediction of the Sleipner CO₂ Plume from 2006 to
616 2012. *In: Dixon, T. and Yamaji, K. (eds) Energy Procedia*. Proceedings of the 11th International
617 Conference on Greenhouse Gas Control Technologies, 18-22 November 2012, Kyoto, Japan, **37**, 3529-
618 3545, <https://doi.org/10.1016/j.egypro.2013.06.246>
619
- 620 Cavanagh, A. J. and Haszeldine, R. S. 2014. The Sleipner storage site: Capillary flow modeling of a
621 layered CO₂ plume requires fractured shale barriers within the Utsira Formation. *International Journal*
622 *of Greenhouse Gas Control*, **21**, 101-112, <https://doi.org/10.1016/j.ijggc.2013.11.017>
623
- 624 Chadwick, R. A. 2013. Offshore CO₂ storage: Sleipner natural gas field beneath the North Sea. *In:*
625 Gluyas, J. and Mathias, S. (eds.) *Geological Storage of Carbon Dioxide (CO₂)*. Woodhead, 227-250,
626 <https://doi.org/10.1533/9780857097279.3.227>
627
- 628 Eiken, O., Ringrose, P., Hermanrud, C., Nazarian, B., Torp, T. and Høier, L. 2011. Lessons learned from
629 14 years of CCS operations: Sleipner, In Salah and Snøhvit. *In: Gale, J., Hendriks, C. and Turkenberg,*
630 *W. (eds) Energy Procedia*. 10th International Conference on Greenhouse Gas Control Technologies,
631 19-23 September 2010, Amsterdam, The Netherlands, **4**, 5541-5548,
632 <https://doi.org/10.1016/j.egypro.2011.02.541>
633
- 634 Gilfillan, S. M. V., Ballentine, C. J., Holland, G., Blagburn, D., Sherwood Lollar, B., Stevens, S., Schoell,
635 M. and Cassidy, M. 2008. The noble gas geochemistry of natural CO₂ gas reservoirs from the Colorado
636 Plateau and Rocky Mountain provinces, USA. *Geochimica et Cosmochimica Acta*, **72**, 1174-1198,
637 <https://doi.org/10.1016/j.gca.2007.10.009>
638
- 639 Gilfillan, S. M. V., Sherwood Lollar, B., Holland, G., Blagburn, D., Stevens, S., Schoell, M., Cassidy, M.,
640 Ding, Z., Zhou, Z., Lacrampe-Couloume, G. and Ballentine, C. J. 2009. Solubility trapping in formation
641 water as dominant CO₂ sink in natural gas fields. *Nature*, **458**, 614-618,
642 <https://doi.org/10.1038/nature07852>
643
- 644 Gilmore, K. A., Neufeld, J. A. and Bickle, M. J. 2020. CO₂ Dissolution Trapping Rates in Heterogenous
645 Porous Media. *Geophysical Research Letters*, **47**, e2020GL087001,
646 <https://doi.org/10.1029/2020GL087001>
647
- 648 Haszeldine, R. S., Quinn, O., England, G., Wilkinson, M., Shipton, Z. K., Evans, J. P., Heath, J., Crossey,
649 L., Ballentine, C. J. and Graham, C. M. 2005. Natural Geochemical Analogues for Carbon Dioxide
650 Storage in Deep Geological Porous Reservoirs, a United Kingdom Perspective. *Oil & Gas Science and*
651 *Technology*, **60**, 33–49, <https://doi.org/10.2516/ogst:2005004>
652
- 653 Holland, G. and Gilfillan, S. 2013. Application of Noble Gases to the Viability of CO₂ Storage. *In:* Burnard
654 P. (ed.) *The Noble Gases as Geochemical Tracers. Advances in Isotope Geochemistry*. Springer, 177-
655 223, https://doi.org/10.1007/978-3-642-28836-4_8
656

- 657 Jacob, R. and Saylor, B. Z. 2016. CO₂ solubility in multi-component brines containing NaCl, KCl, CaCl₂
 658 and MgCl₂ at 297 K and 1-14 MPa. *Chemical Geology*, **424**, 86-95,
 659 <https://doi.org/10.1016/j.chemgeo.2016.01.013>
 660
- 661 Kempka, T., De Lucia, M. and Kühn, M. 2014. Geomechanical integrity verification and mineral
 662 trapping quantification for the Ketzin CO₂ storage pilot site by coupled numerical simulations. *In:*
 663 Dixon, T., Herzog, H. and Twining, S. (eds) *Energy Procedia*. 12th International Conference on
 664 Greenhouse Gas Control Technologies, 5-9 October 2014, Austin, USA, **63**, 3330-3338,
 665 <https://doi.org/10.1016/j.egypro.2014.11.361>
 666
- 667 Martinez, M. J. and Hesse M. A. 2016. Two-phase convective CO₂ dissolution in saline aquifers. *Water*
 668 *Resources Research*, **52**, 585-599, <https://doi.org/10.1002/2015WR017085>
 669
- 670 Majer, V., Sedlbauer, J. and Bergin, G. 2008. Henry's law constant and related coefficients for aqueous
 671 hydrocarbons, CO₂ and H₂S over a wide range of temperature and pressure. *Fluid Phase Equilibria*,
 672 **272**, 65-74, <https://doi.org/10.1016/j.fluid.2008.07.013>
 673
- 674 Miocic, J. M., Gilfillan, S. M. V., Roberts, J. J., Edlmann, K., McDermott, C. I. and Haszeldine R. S.
 675 Controls on CO₂ storage security in natural reservoirs and implications for CO₂ storage site selection.
 676 *International Journal of Greenhouse Gas Control*, **51**, 118-125,
 677 <https://doi.org/10.1016/j.ijggc.2016.05.019>
 678
- 679 Nereson, A., Stroud, J., Karlstrom, K., Heizler, M. and McIntosh, W. 2013. Dynamic topography of the
 680 western Great Plains: Geomorphic and 40Ar/39Ar evidence for mantle-driven uplift associated with
 681 the Jemez lineament of NE New Mexico and SE Colorado. *Geosphere*, **9**, 521-545,
 682 <https://doi.org/10.1130/GES00837.1>
 683
- 684 Newmark, R. L., Friedmann, S. J. and Carrol, S. A. 2010. Water Challenges for Geologic Carbon Capture
 685 and Sequestration. *Environmental Management*, **46**, 651-661, [https://doi.org/10.1007/s00267-010-](https://doi.org/10.1007/s00267-010-9434-1)
 686 [9434-1](https://doi.org/10.1007/s00267-010-9434-1)
 687
- 688 Nooner, S. L., Eiken, O., Hermanrud, C., Sasagawa, G. S., Stenvold, T. and Zumberge, M. A. 2007.
 689 Constraints on the *in situ* density of CO₂ within the Utsira formation from time-lapse seafloor gravity
 690 measurements. *International Journal of Greenhouse Gas Control*, **1**, 198-214,
 691 [https://doi.org/10.1016/S1750-5836\(07\)00018-7](https://doi.org/10.1016/S1750-5836(07)00018-7)
 692
- 693 Orsini, P., Cantucci, B. and Quattrocchi, F. 2014. Large-scale Numerical Modelling of CO₂ Injection and
 694 Containment Phases for an Italian Near-coast Reservoir Using PFLOTRAN. *In:* Røkke, N, A. and
 695 Svendsen, H. (eds) *Energy Procedia*. 7th Trondheim Conference on CO₂ capture, Transport and
 696 Storage, 4-6 June 2013, Trondheim, Norway, **51**, 334-343,
 697 <https://doi.org/10.1016/j.egypro.2014.07.040>
 698
- 699 Ozah, R. C., Lakshminarasimhan, S., Pope, G. A., Sepehrnoori, K., and Bryant, S. L. 2005. Numerical
 700 Simulation of the Storage of Pure CO₂ and CO₂-H₂S Gas Mixtures in Deep Saline Aquifers. Paper SPE
 701 97255, presented at the SPE Annual Technical Conference and Exhibition, 9-12 October 2005, Dallas,
 702 USA, <https://doi.org/10.2118/97255-MS>
 703
- 704 Pickup, G. E., Jin, M., Olden, P., Mackay, E. J. and Sohrabi, M. 2011. A Sensitivity Study on CO₂ Storage
 705 in Saline Aquifers. Paper SPE 143054, presented at the SPE EUROPEC/EAGE Annual Conference and
 706 Exhibition, 23-26 May 2011, Vienna, Austria, <https://doi.org/10.2118/143054-MS>
 707

- 708 Pruess, K. and Nordbotten, J. 2011. Numerical Simulation Studies of the Long-term Evolution of a CO₂
 709 Plume in a Saline Aquifer with a Sloping Caprock. *Transport in Porous Media*, **90**, 135-151,
 710 <https://doi.org/10.1007/s11242-011-9729-6>
 711
- 712 Pruess, K. and Spycher, N. 2007. ECO₂N - A fluid property module for the TOUGH2 code for studies of
 713 CO₂ storage in saline aquifers. *Energy Conversion and Management*, **48**, 1761-1767,
 714 <https://doi.org/10.1016/j.enconman.2007.01.016>
 715
- 716 Riaz, A. and Cinar, Y. 2014. Carbon dioxide sequestration in saline formations: Part I-Review of the
 717 modeling of solubility trapping. *Journal of Petroleum Science and Engineering*, **124**, 367-380,
 718 <https://doi.org/10.1016/j.petrol.2014.07.024>
 719 Rohatgi, A. 2020. WebPlotDigitizer version 4.3,
 720 <https://automeris.io/WebPlotDigitizer>
- 721 Sathaye, K. J., Hesse, M. A., Cassidy, M. and Stockli, D. F. 2014. Constraints on the magnitude and rate
 722 of CO₂ dissolution at Bravo Dome natural gas field. *Proceedings of the National Academy of Sciences*
 723 *of the United States of America*, **43**, 15332-15337, <https://doi.org/10.1073/pnas.1406076111>
 724
- 725 Sathaye, K. J., Smye, A. J., Jordan, J. S. and Hesse, M. A. 2016. Noble gases preserve history of retentive
 726 continental crust in the Bravo Dome natural CO₂ field, New Mexico. *Earth and Planetary Science*
 727 *Letters*, **443**, 32-40, <https://doi.org/10.1016/j.epsl.2016.03.014>
 728
- 729 Sato, K., Mito, S., Horie, T., Ohkuma, H., Saito, H., Watanabe, J. and Yoshimura, T. 2011. Monitoring
 730 and simulation studies for assessing macro- and meso-scale migration of CO₂ sequestered in an
 731 onshore aquifer: Experiences from the Nagaoka pilot site, Japan. *International Journal of Greenhouse*
 732 *Gas Control*, **5**, 125-137, <https://doi.org/10.1016/j.ijggc.2010.03.003>
 733
- 734 Soltanian M. R., Amooie, M. A., Gershenson, N., Dai, Z., Ritzi, R., Xiong, F., Cole, D. and Moortgat, J.
 735 2017. Dissolution Trapping of Carbon Dioxide in Heterogeneous Aquifers, *Environmental Science &*
 736 *Technology*, **51**, 7732-7741, <https://doi.org/10.1021/acs.est.7b01540>
 737
- 738 Spycher, N. and Pruess, K. 2005. CO₂-H₂O mixtures in the geological sequestration of CO₂. II.
 739 Partitioning in chloride brines at 12-100°C and up to 600 bar. *Geochimica et Cosmochimica Acta*, **69**,
 740 3309-3320, <https://doi.org/10.1016/j.gca.2005.01.015>
 741
- 742 Steel, L., Liu, K., Mackay, E. and Maroto-Valer, M. M. 2016. CO₂ solubility measurements in brine under
 743 reservoir conditions: A comparison of experimental and geochemical modeling methods. *Greenhouse*
 744 *Gas Science and Technology*, **6**, 197-217, <https://doi.org/10.1002/ghg.1590>
 745
- 746 Szulczewski, M. L., Hesse, M. A. and Juanes, R. 2013. Carbon dioxide dissolution in structural and
 747 stratigraphic traps. *Journal of Fluid Mechanics*, **736**, 287-315, <https://doi.org/10.1017/jfm.2013.511>
 748
- 749 Williams, G. A. and Chadwick, R. A. 2021. Influence of reservoir-scale heterogeneities on the growth,
 750 evolution and migration of a CO₂ plume at the Sleipner Field, Norwegian North Sea. *International*
 751 *Journal of Greenhouse Gas Control*, **106**, 103260, <https://doi.org/10.1016/j.ijggc.2021.103260>
 752
- 753 Wycherley, H., Fleet, A. and Shaw, H. 1999. Some observations on the origins of large volumes of
 754 carbon dioxide accumulations in sedimentary basins. *Marine and Petroleum Geology*, **16**, 489-494,
 755 [https://doi.org/10.1016/S0264-8172\(99\)00047-1](https://doi.org/10.1016/S0264-8172(99)00047-1)
 756

757 Zhou, Z., Ballentine, C. J., Schoell, M. and Stevens, S. H. 2012. Identifying and quantifying natural CO₂
 758 sequestration processes over geological timescales: The Jackson Dome CO₂ Deposit, USA. *Geochimica*
 759 *et Cosmochimica Acta*, **86**, 257-275, <https://doi.org/10.1016/j.gca.2012.02.028>

760
 761 Zwahlen, C, A., Kampman, N., Dennis, P., Zhou, Z. and Holland, G. 2017. Estimating carbon dioxide
 762 residence time scales through noble gas and stable isotope diffusion profiles. *Geology*, **45**, 995-998,
 763 <https://doi.org/10.1130/G39291.1>

764
 765 **Figure captions**

766
 767 **Fig. 1:** Alternative scenarios for the evolution of CO₂ dissolution rate (orange) and cumulative CO₂
 768 dissolution (blue) in storage reservoirs: (a) Dissolution rates are high during the injection phase and
 769 decline rapidly; dissolution rates are low in the post-injection phase and decline to zero when
 770 equilibrium is reached. (b) Dissolution rates are high during the injection phase but decline less rapidly
 771 and continue after stabilisation of the CO₂ plume. This requires the occurrence of significant
 772 dissolution across the gas-water contact by diffusion and potentially convection. The expected
 773 injection duration is decades. The storage duration would extend to 10⁴ to 10⁶ years depending on the
 774 specific case study and underlying assumptions.

775
 776 **Fig. 2:** Schematic of CO₂-water interactions during dissolution. (a) The reservoir is charged with CO₂
 777 and trace gases including ³He. The formation water contains ⁴He and ²⁰Ne that are not present in the
 778 CO₂. (b) CO₂ dissolves into the formation water and ⁴He and ²⁰Ne partition into the CO₂ at varying rates
 779 across the reservoir. (c) Gas sampled from wells establishes the relative CO₂ removal. ⁴He and ²⁰Ne
 780 establish the formation water-CO₂ interactions. In this example, lower rates of dissolution in well 1
 781 are evidenced by higher CO₂/³He and lower ⁴He and ²⁰Ne concentrations relative to well 2.

782
 783 **Fig. 3:** Fraction of total CO₂ dissolved over duration of simulation or residence time. The data groups
 784 into three trends: (a) high rates and high impacts, resulting in 60% to 80% dissolution within a few
 785 thousand years; (b) moderate rates and impacts, resulting in 30% to 40% dissolution within tens of
 786 thousands of years; and (c) low rates and impacts, resulting in less than 20% dissolved within a
 787 hundred thousand years. Best-fit lines, dashed, are approximate and plot as exponential decay curves
 788 in non-log space. Bravo Dome studies and Kempka *et al.* (2014) model include min-max ranges.
 789 Sleipner gravity inversion (Alnes *et al.* 2011); Bravo Dome geochemistry (Sathaye *et al.* 2014; Zwahlen
 790 *et al.* 2017); and selected simulation case studies (Ozah *et al.* 2005; Pickup *et al.* 2011; Pruess &
 791 Nordbotten 2011; Sato *et al.* 2011; Bonneville *et al.* 2013; Kempka *et al.* 2014; Orsini *et al.* 2014).

792
 793 **Fig. 4:** Fraction of total injected, simulated, or emplaced CO₂ dissolved per year, plotted against total
 794 simulation or residence time. The circle areas are scaled to the total mass of CO₂ in each study. A
 795 minimum point size is applied to make the position of Pruess & Nordbotten (2011), Sato *et al.* (2011)
 796 and Kempka *et al.* (2014) visible. The dashed trend lines represent a log-log gradient for a 10x
 797 reduction in average dissolution rate with a corresponding 10x increase in storage time. The high
 798 dissolution trend represents 100% of CO₂ dissolving. This is equivalent to 10x the average annual
 799 dissolution rate for CO₂ at Sleipner (Alnes *et al.* 2011). The low dissolution trend, representing 10% of
 800 CO₂ dissolving, is approximately equivalent to the average annual Sleipner rate.

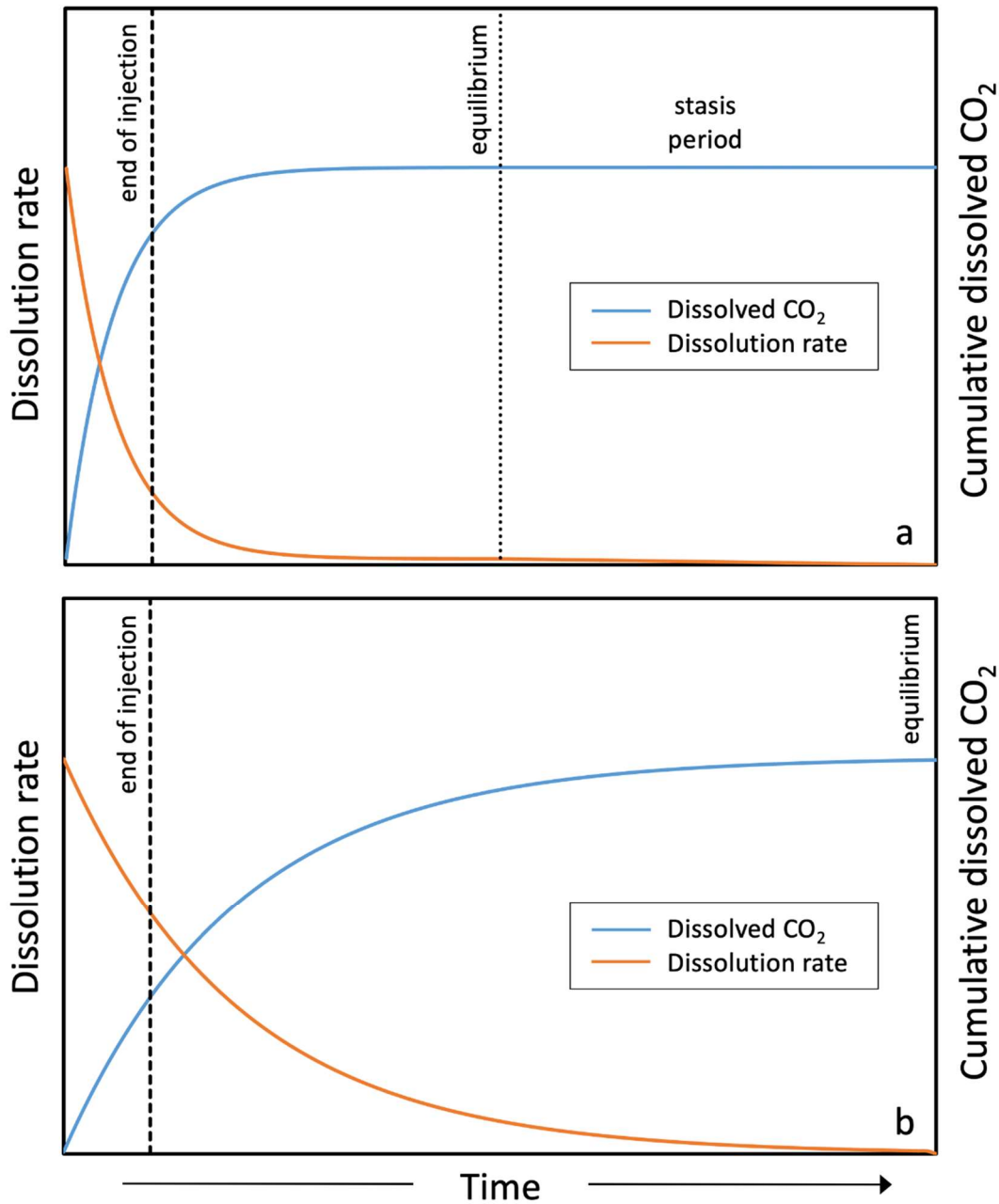
801
 802 **Fig. 5:** Linear time plot of average dissolution rate for all studies excluding the near-field and far-field
 803 outliers (Sleipner, Bonneville *et al.* (2013) and 'old' Bravo Dome). When treated as a single population,
 804 the exponential trend line has a poor correlation (R² < 0.7). The coefficient of determination improves
 805 (R² > 0.95) when the case studies are grouped as high and moderate rate populations. At t₀, the high-
 806 rate trend is equal to 0.07%, under predicting the average Sleipner rate, 0.9%, by a factor of 13. In the

807 far-field to the right of the plot, at 100 kyr, the bridge point between ‘young’ and ‘old’ Bravo Dome
 808 models, the fraction of CO₂ dissolved per year has decayed to less than 10⁻¹⁰ for all trend lines.
 809

810 **Fig. 6:** Dissolution rates over time (a) in log-log domain, and (b) plotted linearly for the first 5.5 kyr.
 811 Note the deviation of Bonneville *et al.* (2013) from a constant log-log gradient, indicating a rapid
 812 decline in dissolution within 100 years. For Sathaye *et al.* (2014), both the initial rate to 5 kyr and the
 813 long-term rate to 1.2–1.5 Ma are shown. Plotted studies: Sleipner (Alnes *et al.* 2011); Bravo Dome
 814 (Sathaye *et al.* 2014; Zwhalen *et al.* 2017). Simulations: Ozah *et al.* 2005; Pruess & Nordbotten 2011;
 815 Sato *et al.* 2011; Bonneville *et al.* 2013; Kempka *et al.* 2014. Analytical: Szulczewski *et al.* 2013.
 816

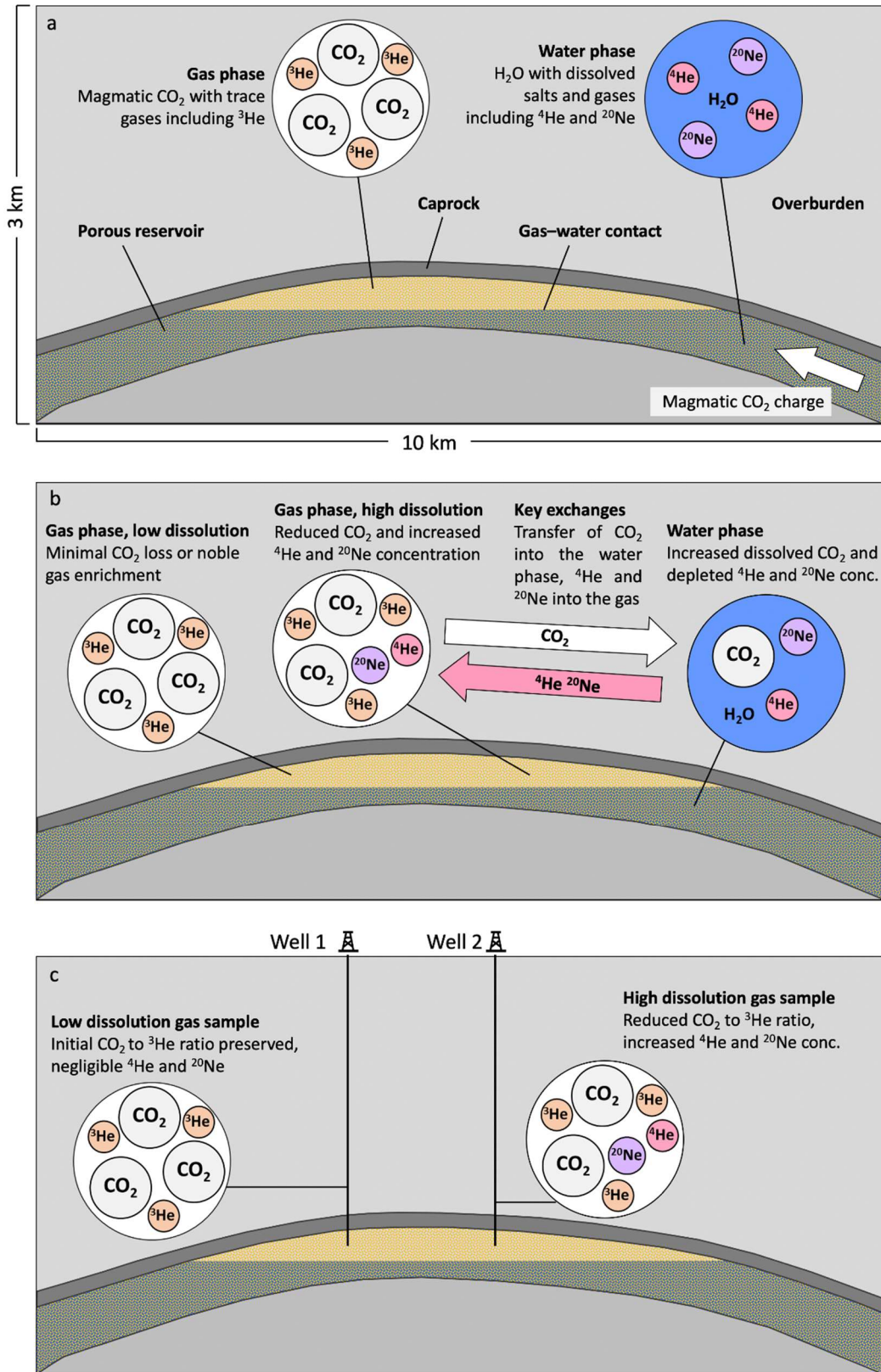
817 **Figures**

818
 819 **Fig. 1**



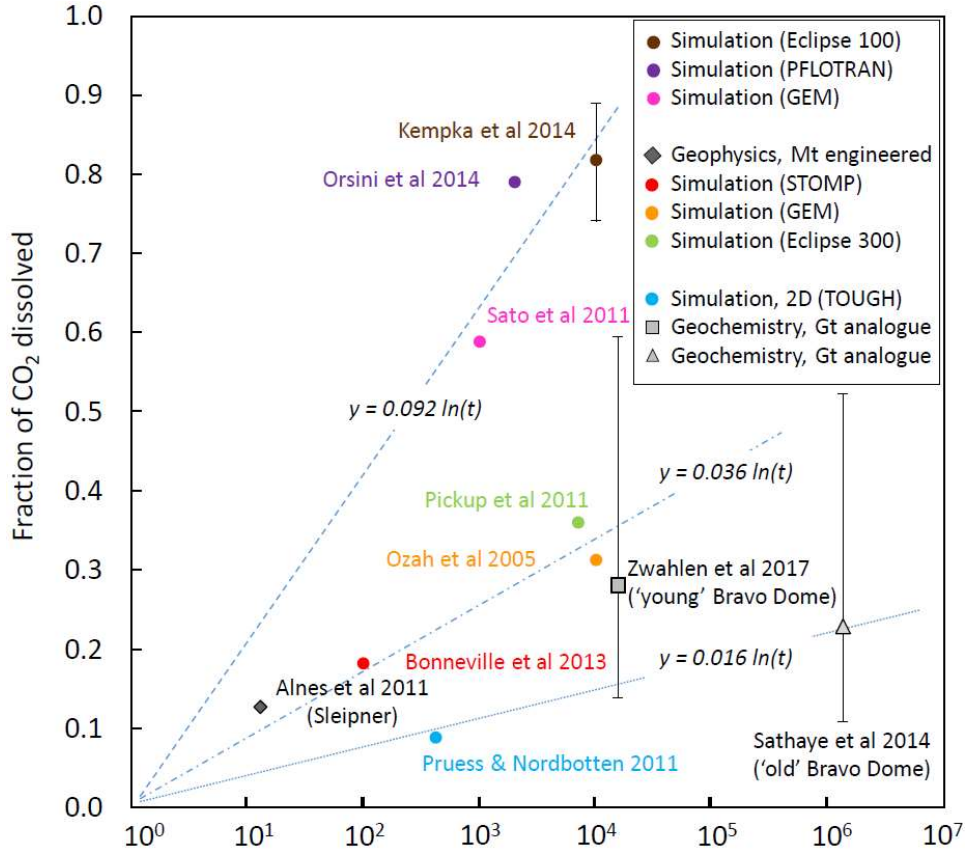
820
 821

822 **Fig. 2**
 823
 824

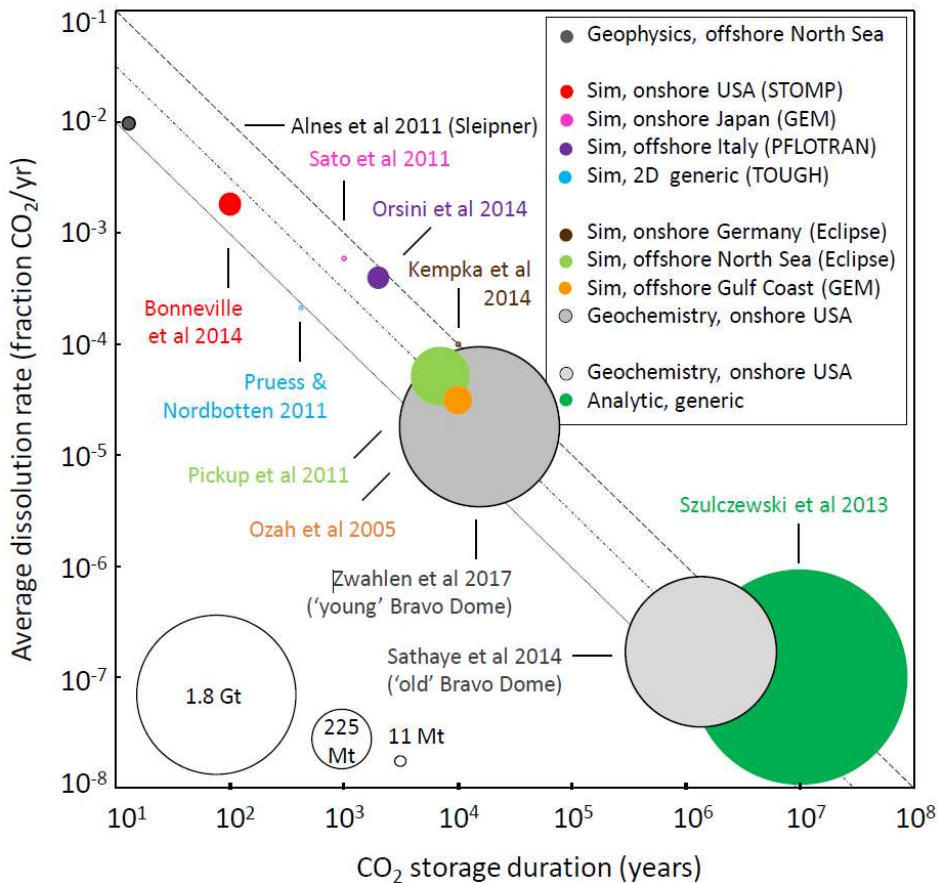


825
 826
 827
 828

829 Fig. 3

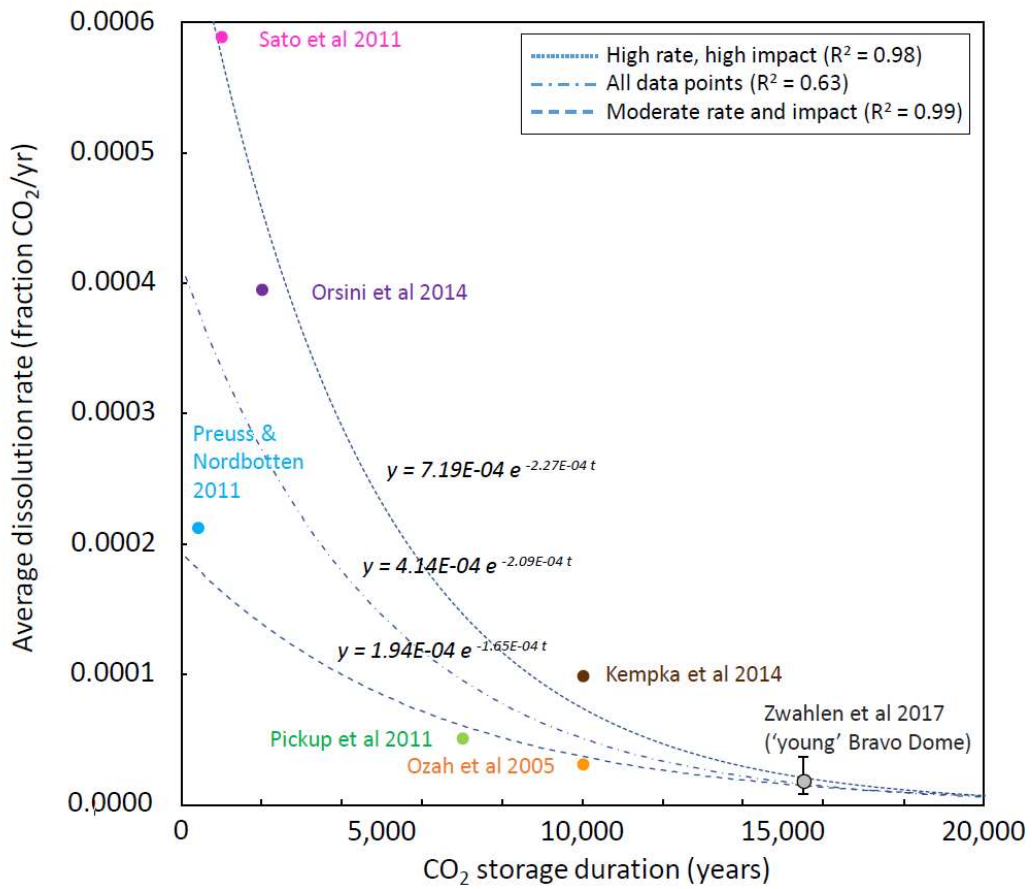


830
831
832 Fig. 4

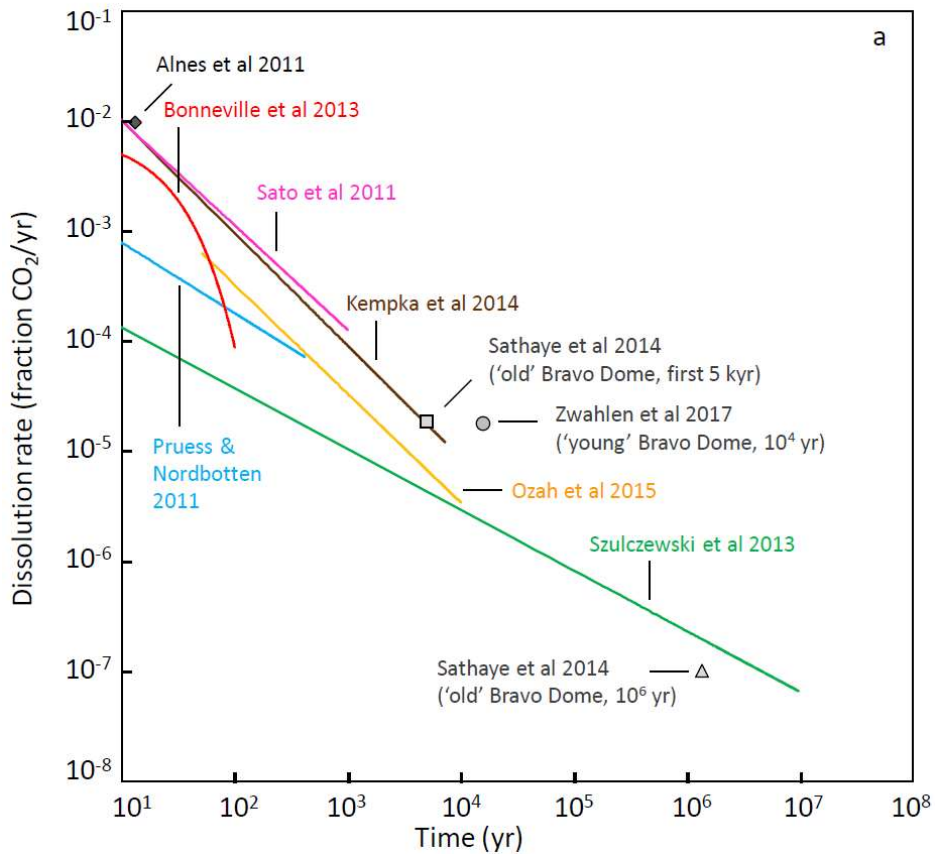


833

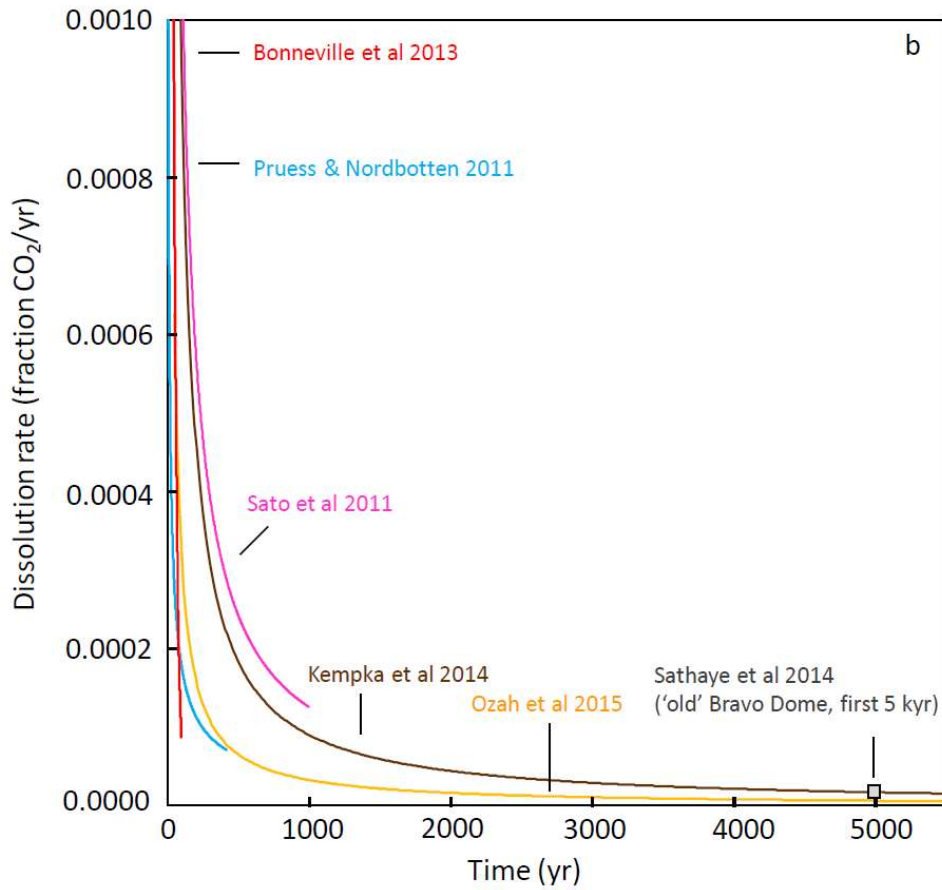
834 Fig. 5



835 Fig. 6
836



837



838
839
840
841
842
843

Tables

Table 1: CO₂ dissolution mass, age and rate estimates for Bravo Dome analogue studies

Bravo Dome Publications	Emplaced CO ₂ (Mt)	Dissolved CO ₂ (Mt)	Estimated Fraction Dissolved	Age of CO ₂ emplacement	Dissolution rate (Mt/kyr)*
Sathaye <i>et al.</i> (2014)	1600 ± 670	366 ± 120	0.11 – 0.52	1.2 – 1.5 Ma	0.3
Zwahlen <i>et al.</i> (2017)	1800 ± 670	506 ± 166	0.14 – 0.59	14 – 17 ka	32.6

844 *Mid-point of age estimates used

845
846
847

Table 2: Case studies and simulations summary

Publication	Approach	Location and Setting	CO ₂ Mass (Mt)	Fraction Dissolved	Model/CO ₂ storage duration (yr)	Fraction CO ₂ dissolved /yr
Ozah <i>et al.</i> 2005	Simulation - GEM	Generic Gulf Coast saline aquifer, USA	48.0	0.31	10000	3.13 x 10 ⁻⁵
Pickup <i>et al.</i> 2011	Simulation - Eclipse 300	Sherwood Formation, East Irish Sea, UK	225	0.36	7000	5.14 x 10 ⁻⁵

Pruess & Nordbotten 2011	Simulation - TOUGH2	Generic Continental USA	0.160	0.09	418	2.12×10^{-4}
Sato <i>et al.</i> 2011	Simulation - GEM	Nagaoka pilot site; Haizume Formation, Japan	0.010	0.59	1000	5.89×10^{-4}
Bonneville <i>et al.</i> 2013	Simulation - STOMP-CO2	Proposed FutureGen 2.0 site; Mt Simon Formation, Illinois, USA	33.0	0.18	100	1.82×10^{-3}
Szulczewski <i>et al.</i> 2013	Analytical model	Generic aquifer	3214*		10000000	1.00×10^{-7}
Kempka <i>et al.</i> 2014	Simulation - ECLIPSE100	Ketzin pilot site; Stuttgart Formation, Germany	0.067	0.89	10000	8.92×10^{-5}
Orsini <i>et al.</i> 2014	Simulation - PFLOWTRAN	Carbonate aquifer, offshore Italy	30.0	0.79	2000	3.95×10^{-4}
Alnes <i>et al.</i> 2011	Gravimetric survey	Sleipner pilot site, Utsira Formation, North Sea, Norway	11.3	0.13	13	9.69×10^{-3}
Sathaye <i>et al.</i> 2014	Isotope geochemistry	Bravo Dome, New Mexico, USA	1600	0.23	1350000	1.69×10^{-7}
Zwahlen <i>et al.</i> 2017	Isotope geochemistry	Bravo Dome, New Mexico, USA	1800	0.28	15500	1.81×10^{-5}

848 *Model uses constant supply of CO₂ above the reservoir. The CO₂ mass value is equal to the mass of
849 CO₂ dissolved into the reservoir